Numerical Simulation of Resonant Tunneling Diodes with a Quantum-Drift-Diffusion Model

Stefano Micheletti[1], Riccardo Sacco[1], and Paolo Simioni

MOX - Modeling and Scientific Computing, Dipartimento di Matematica "F. Brioschi", Politecnico di Milano, via Bonardi 9, I-20133 Milano, Italy

Abstract. We deal with a Quantum-Drift-Diffusion (QDD) model for the description of transport in semiconductors which generalizes the standard Drift-Diffusion model (DD) through extra terms that take into account some quantum dispersive corrections. We also study numerically the influence on the I-V curve of the electron effective mass, the barrier height and width, and of the ambient temperature. The performance of several linearization algorithms, i.e. a two Gummel-type iterations and the fully-coupled Newton method are also compared.

1 The QDD Model

The unipolar QDD model for a semiconductor occupying the open bounded region $\Omega \subset \mathbb{R}^d$, $d = 1, 2, 3$, comprises the following set of equations in the space-time cylinder $\Omega \times (0, t_f]$:

$$\begin{cases} \dfrac{\partial n}{\partial t} + \nabla \cdot (\mu n \nabla F) = 0 \ , \\ F = V \underbrace{+ V_{\rm bar}}_{\rm (I)} - V_{\rm th} \ln \dfrac{n}{n_i} \underbrace{+ \dfrac{\hbar^2}{6mq} \dfrac{1}{\sqrt{n}} \nabla^2 \sqrt{n}}_{\rm (II)} \ , \\ \nabla^2 V = \dfrac{q}{\epsilon} (n - N_d) \ , \end{cases} \tag{1}$$

where n is the electron concentration, V the electric potential, F the quasi-Fermi potential, N_d the doping profile, $V_{\rm bar}$ the barrier potential, $V_{\rm th}$ the thermal voltage, n_i the electron intrinsic concentration, μ the mobility, while the quantities $\hbar, q, \epsilon, m$ are the reduced Planck constant, the (positive) electron charge, the semiconductor permettivity and the electron effective mass, respectively. The above system, supplemented with suitable initial and boundary conditions, is to be solved for the unknowns n, V, F. The electron current density is given by the constitutive law $\underline{J} = -q\mu n \nabla F$, so that $(1)_1$ represents the classical continuity equation but with a nonclassical constitutive law for the current density. Moreover, like in the DD case, the temperature is supposed to be constant, having neglected all the energetic exchange phenomena. In $(1)_1$-$(1)_3$ we have singled out the two terms that characterize the QDD model with respect to the DD model, i.e.

(I) is the potential due to the presence of the heterostructure corresponding to barriers and wells between the different materials, while
(II) is the dispersive term, modeling a typical quantum effect [1].

The bipolar QDD model has been studied in [7] where the conditions under which existence and uniqueness of the solution at thermodynamic equilibrium hold are discussed, basically, via a variational argument consisting in minimizing the total energy of the system. In nonequilibrium conditions, the uniqueness of the solution is proved to hold only for moderate external voltages ([7]). This fact has a real counterpart in RTD's which exhibit a hysteresis cycle for particular values of the external voltage, as proved experimentally, as well as numerically ([3]).

2 Iterative Maps and Numerical Algorithms

In this section we address both the linearization techniques and the numerical issues necessary to obtain an approximate solution to the QDD equations.

2.1 Iterative Maps

To solve the (nonlinear) system $(1)_1$-$(1)_3$ it is necessary to employ some linearization techniques. In particular, we have compared three different functional iterative algorithms:

1. The fully-coupled Newton method;
2. A two-step fixed-point map for F which can be summed up as: Given $F^{(k)}, V^{(k)}, n^{(k)}$, first
   - solve $(1)_2$-$(1)_3$ for $n^{(k+1)}, V^{(k+1)}$ with coupled Newton's method, then
   - solve the (linear) equation $(1)_1$ for $F^{(k+1)}$;
3. A three-step generalized Gummel's map such that: Given $F^{(k)}, V^{(k)}, n^{(k)}$
   - solve the (nonlinear) equation $(1)_2$ for $n^{(k+1)}$, then
   - solve the nonlinear version of $(1)_3$ for $V^{(k+1)}$

$$\nabla^2 V^{(k+1)} = \frac{q}{\epsilon}\left(n^{(k+1)} \exp\left(\frac{V^{(k+1)} - V^{(k)}}{V_{\mathrm{th}}}\right) - N_{\mathrm{d}}\right) \quad , \text{ finally}$$

   - solve the (linear) equation $(1)_1$ for $F^{(k+1)}$.

The three algorithms above are ordered in decreasing degree of coupling: algorithm 1. is a very well-known general purpose method, algorithm 2. is theoretically and numerically studied in [7], whereas algorithm 3. is our novel contribution, first devised in [8]. This last algorithm generalizes the classical Gummel map to the QDD model, whereby three successive subproblems are to be solved at each step. In particular, it consists of two nonlinear steps for $n^{(k+1)}$ and $V^{(k+1)}$, respectively, and a linear step for $F^{(k+1)}$. We have applied the three algorithms to the solution of a RTD and some numerical

results are shown in Sect. 3. Hereafter, we shall study the stationary QDD model, i.e. we shall assume $\frac{\partial \cdot}{\partial t}$ for all the variables. Let us dwell on algorithm 3. which can be considered as a generalized Gummel map, see e.g. [4]. From $(1)_2$ and letting $\alpha = \frac{\hbar^2}{6mq}$, we have $n = n_{\rm i} \exp\left(\frac{\alpha \frac{1}{\sqrt{n}} \nabla^2 \sqrt{n} + V + V_{\rm bar} - F}{V_{\rm th}}\right)$, and substituting in $(1)_3$, we obtain

$$\nabla^2 V = \frac{q}{\epsilon}\left(n_{\rm i} \exp\left(\frac{\alpha \frac{1}{\sqrt{n}} \nabla^2 \sqrt{n} + V_{\rm bar}}{V_{\rm th}}\right) \exp \frac{V - F}{V_{\rm th}} - N_{\rm d}\right) \quad , \tag{2}$$

which is the nonlinear version of the Poisson equation. Given $V^{(k)}, F^{(k)}$, $k \geq 0$, the first step of the algorithm consists in solving the following boundary value problem for $n = n^{(k+1)}$

$$\begin{cases} \alpha \dfrac{1}{\sqrt{n}} \nabla^2 \sqrt{n} - V_{\rm th} \ln \dfrac{n}{n_{\rm i}} + V_{\rm bar} + V^{(k)} - F^{(k)} = 0 \text{ in } \Omega \ , \\ n = n_{\rm eq} \qquad\qquad\qquad\qquad\qquad\qquad \text{on } \Gamma_{\rm D} \ , \\ \nabla n \cdot \underline{\nu} = 0 \qquad\qquad\qquad\qquad\qquad\qquad \text{on } \Gamma_{\rm N} \ , \end{cases} \tag{3}$$

where $n_{\rm eq}$ is the equilibrium value of the concentration, while $\Gamma_{\rm D}, \Gamma_{\rm N}$ are two subsets of the boundary $\partial\Omega$ such that $\partial\Omega = \overline{\Gamma}_{\rm D} \cup \overline{\Gamma}_{\rm N}$, with $\Gamma_{\rm D} \neq \emptyset$, and $\underline{\nu}$ is the unit outward normal vector to $\partial\Omega$. Then from (3) we formally obtain $V_{\rm th} \ln \frac{n^{(k+1)}}{n_{\rm i}} - V^{(k)} + F^{(k)} = \alpha \frac{1}{\sqrt{n^{(k+1)}}} \nabla^2 \sqrt{n^{(k+1)}} + V_{\rm bar}$, which used in (2) allows us to write the second step of the algorithm, to solve for $V = V^{(k+1)}$, as

$$\begin{cases} \nabla^2 V = \dfrac{q}{\epsilon}\left(n^{(k+1)} \exp\left(\dfrac{V - V^{(k)}}{V_{\rm th}}\right) - N_{\rm d}\right) \text{ in } \Omega \ , \\ V = V_{\rm eq} + V_{\rm ext} \qquad\qquad\qquad\qquad \text{on } \Gamma_{\rm D} \ , \\ \nabla V \cdot \underline{\nu} = 0 \qquad\qquad\qquad\qquad\qquad\qquad \text{on } \Gamma_{\rm N} \ , \end{cases} \tag{4}$$

where $V_{\rm eq}, V_{\rm ext}$ are the equilibrium value of the potential and the external applied voltage, respectively. We point out that this equation can be regarded as the QDD counterpart of the DD nonlinear Poisson equation for V, i.e.

$$\nabla^2 V = \frac{q}{\epsilon}\left(n_{\rm i} \exp\left(\frac{V - F}{V_{\rm th}}\right) - N_{\rm d}\right) \quad ,$$

where $n_{\rm i}$ is replaced by $n^{(k+1)} \exp\left(\frac{F^{(k)} - V^{(k)}}{V_{\rm th}}\right)$. Finally, the last step of the algorithm requires solving the linear problem for $F = F^{(k+1)}$

$$\begin{cases} \nabla \cdot (\mu n^{(k+1)} \nabla F) = 0 \text{ in } \Omega \ , \\ F = F_{\rm eq} + V_{\rm ext} \qquad \text{on } \Gamma_{\rm D} \ , \\ \nabla F \cdot \underline{\nu} = 0 \qquad\qquad \text{on } \Gamma_{\rm N} \ , \end{cases} \tag{5}$$

where $F_{\rm eq}$ is the equilibrium value of the quasi-Fermi level. The sequence of problems (3)-(5) defines our version of the Gummel map applied to the

iterative solution of the QDD model. We remark that the nonlinear steps (3)-(4) are both linearized with Newton's method. Moreover, computationally, it is advantageous to solve problem (3) for $w = \sqrt{n}$ instead of n, which yields the following problem for $w = w^{(k+1)}$

$$\begin{cases} \alpha\nabla^2 w - 2V_{\rm th} w \ln\dfrac{w}{w_{\rm i}} + w(V_{\rm bar} + V^{(k)} - F^{(k)}) = 0 \text{ in } \Omega \ , \\ w = w_{\rm eq} \qquad\qquad\qquad\qquad\qquad\qquad \text{on } \Gamma_{\rm D} \ , \\ \nabla w \cdot \underline{\nu} = 0 \qquad\qquad\qquad\qquad\qquad\qquad \text{on } \Gamma_{\rm N} \ , \end{cases} \tag{6}$$

where $w_{\rm i} = \sqrt{n_{\rm i}}$ and $w_{\rm eq} = \sqrt{n_{\rm eq}}$.

2.2 Numerical Algorithms

As far as the discretization is concerned, all of the three subproblems (6), (4)-(5), after linearization, are solved using piecewise linear finite elements. Special care is necessary for (5) which requires using piecewise harmonic averages for the terms $\mu n^{(k+1)}$. Important issues to deal with are the scaling of the unknowns and the computational cost required to solve all of the algebraic systems arising after the discretization. With reference to a one-dimensional finite element mesh whose characteristic size is h, the following scaling has been used throughout:

$$\overline{n} = Nh^4 \ , \qquad \overline{V} = 10^{-2}\frac{\alpha}{h^2}\sqrt{\frac{\overline{n}}{N}} \ , \qquad \overline{F} = \overline{V} \ ,$$

where N is the value of the doping at the contacts. We have carried out an extensive numerical validation which proves that this scaling guarantees better conditioning of the algebraic linear systems and more equilibrated coefficient matrices. Finally, to compare the three algorithms in terms of computational cost, we have implemented all the numerical codes in Matlab and we have simulated a one-dimensional RTD under different conditions. The results, extensively discussed in [8], show that algorithm 1. is the cheapest one when the sparse structure of the matrices is taken into account, otherwise algorithm 3. performs better. Of course, the algorithms might perform other ways when going to multi-dimensional problems.

3 Numerical Results

We show in this section several numerical results referring to a one-dimensional RTD, i.e. a heterostructure based on two AlGaAs barriers and a quantum GaAs well. The model correctly reproduces the Negative Differential Resistance (NDR) of the I-V characteristic of the device. We aim at studying physical phenomena like the dependence of the I-V characteristics on the electron effective mass, ambient temperature, barrier height and width, as well as to test the numerical algorithms, as already discussed in the previous

section. We have considered a RTD whose geometry is shown in Fig. 1(left): The device length is 75 nm, the doping profile is $5 \times 10^{21}\,\mathrm{m}^{-3}$ in the channel (well and barriers) and $10^{24}\,\mathrm{m}^{-3}$ elsewhere, while all the other parameters vary according to the following simulations. The mobility is assumed to be temperature dependent (cfr. [6]).

Dependence on the Effective Mass

The following figures show some numerical results for a RTD at 77 K. The barrier profile is shown in Fig. 1(right): the height and width are 0.3 V and 5 nm, respectively, while the quantum well is 5 nm wide. Throughout, $J_{\max}, J_{\min}$ denote the current density at the peak and at the valley, respectively, and the Peak to Valley Ratio (PVR) is defined as PVR= $J_{\max}/J_{\min}$. The next four figures in Fig. 2 display the I-V characteristic for the fol-

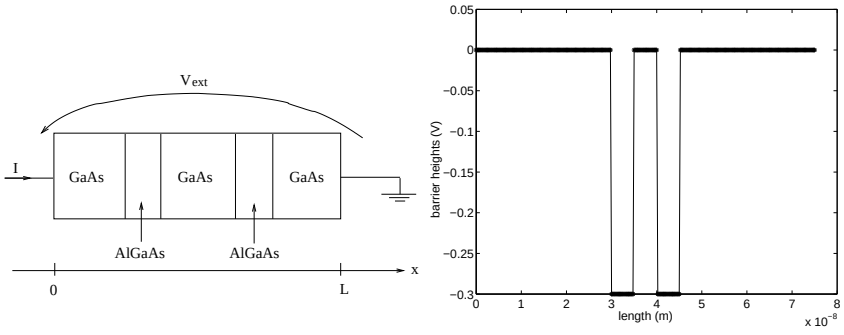

Fig. 1. Geometry (left) and barrier profile (right)

lowing values of the effective mass m (from left to right and top-down): $[0.067, 0.126, 0.1675, 0.201]m_0$, where m_0 is the free-electron mass. Table 1 (left) summarizes the main results. Notice that the higher the effective mass, the stronger the NDR phenomenon, while the PVR increases progressively. Notice that for the lowest value of the effective mass the NDR does not occur. The last pair of figures in Fig. 3 show the electron concentration at the peak and at the valley of the current for the fixed value of the effective mass $m = 0.126m_0$. In particular, notice the large values of the concentration inside the quantum well, especially at the valley which confirm the resonant phenomenon, in accordance with the basic theory of the device ([5]).

Dependence on the Temperature

The second series of simulations is carried out with barrier height and width of 0.35 V and 5 nm, respectively, while the quantum well width is 5 nm and the effective mass is $m = 0.126m_0$. Several values of the ambient tempera-

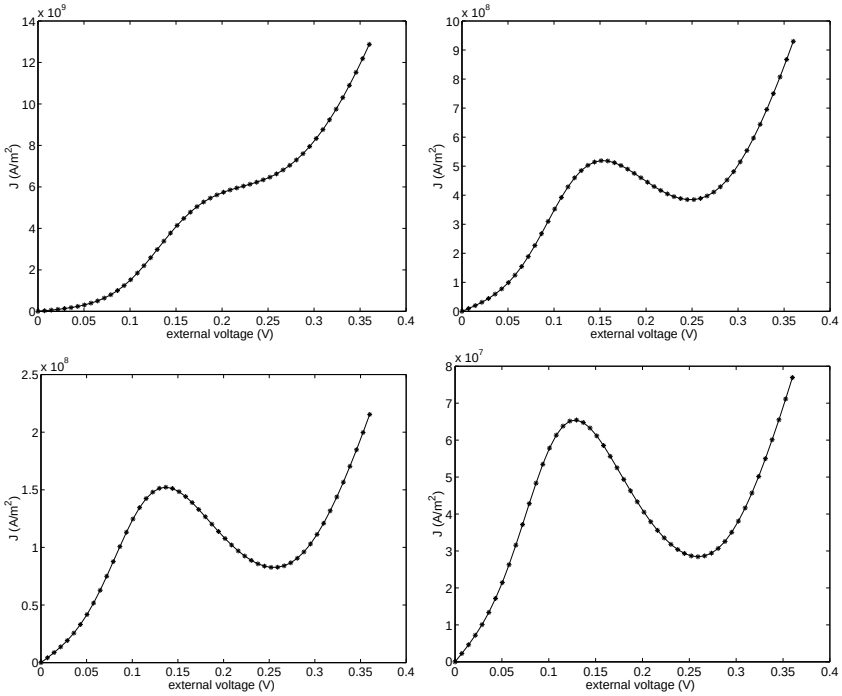

Fig. 2. I-V characteristic: $m = 0.067m_0$ (top left), $m = 0.126m_0$ (top right), $m = 0.1675m_0$ (bottom left) and $m = 0.201m_0$ (bottom right)

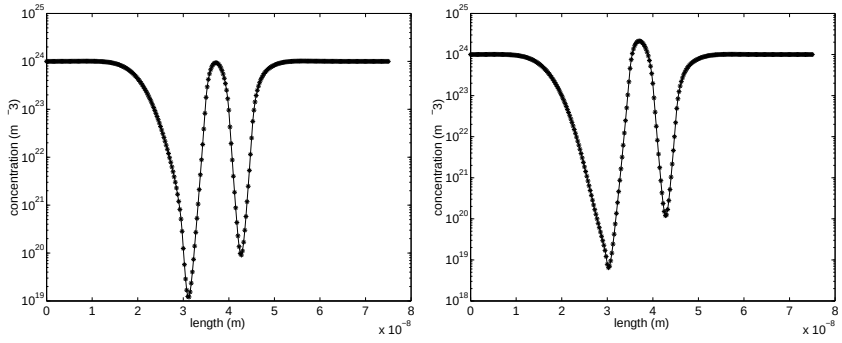

Fig. 3. Electron concentration at the peak (left) and at the valley (right) for $m = 0.126m_0$

ture are considered, i.e. $[77, 100, 150, 200, 300]$ K. Table 1 (right) collects the results (in I.S. units). Observe that the NDR is a typical low temperature phenomenon, weakening as the temperature rises. This behavior can be explained theoretically by considering the different dependence of the current at the valley and at the peak on the temperature. In the first case, the resonant level is inside the energy gap, thus the higher the temperature, the larger the current, because more electrons occupy the energy levels near the conduction band. In the second case, the resonant level coincides with the conduction band, thus the current is less sensitive to the temperature because all the levels near the conduction band have large tunneling probabilities, almost independently of their occupation. As a consequence, the PVR decreases as the temperature rises, until the NDR disappears eventually.

Table 1. I-V characteristics as a function of m (left) and T (right)

$m \times m_0$	$J_{\max} \times 10^8$	$J_{\min} \times 10^8$	PVR
.067	6.22	6.22	//
.126	5.19	3.84	1.35
.1675	1.52	.827	1.84
.201	.654	.284	2.30

T	μ	$J_{\max} \times 10^8$	$J_{\min} \times 10^8$	PVR
77	2.5	2.41	1.23	1.96
100	2.61	3.97	2.6	1.53
150	2.41	9.07	8.45	1.07
200	2.32	20.3	20.3	//

Dependence on the Barrier Height

For this block of simulations we have taken a barrier profile with barrier width of 5 nm and a quantum well width of 5 nm, while the effective mass is $m = 0.126m_0$ and $T = 77$ K. Several values of the barrier height are considered, i.e. $[0.1, 0.2, 0.25, 0.32, 0.4]$ V and the results are summarized in Table 2 (left) (in I.S. units). In this case, the higher the barrier height, the lower the tunneling probability, thus we expect a decrease of the current as the height increases. The PVR should increase with the height because of the contribution to the total current of those electrons drifting thermoionically, which become more important at the valley ([2]).

Dependence on the Barrier Width

For the last series of simulations we have considered a barrier height of 0.325 V, a quantum well width of 5 nm, a fixed device length of 75 nm, an effective mass $m = 0.126m_0$, and $T = 77$ K. The following values of the barrier width have been studied: $[5, 8, 9, 10]$ nm, and Table 2 (right) collects the simulation results (in I.S. units). As the barrier width gets larger the current decreases due to the reduced width of the peak value of the transmission coefficient. Moreover, the PVR, starting with a barrier width equal to the width of the quantum well, should first increase and then decrease ([9]).

Table 2. I-V characteristics at different barrier heights (left) and widths (right)

Height	$J_{\max} \times 10^9$	$J_{\min} \times 10^9$	PVR	Width $\times 10^{-9}$	$J_{\max} \times 10^7$	$J_{\min} \times 10^7$	PVR
0.2	3.23	3.23	//	5	35.0	21.7	1.62
0.25	1.24	1.21	1.03	8	.536	.299	1.79
0.32	.378	.243	1.56	9	.144	.103	1.39
0.4	.12	.041	2.95	10	.041	.037	1.09

4 Conclusions

We have studied and applied the QDD model to the simulation of a RTD. It turns out that the QDD model is able to reproduce typical quantum effects of the device, such as the NDR and correctly reproduces the physical quantities such as electron concentration, electric potential and quasi-Fermi level, even over a wide range of variations of the parameters. We have also carried out a parametric study of the I-V characteristic of the RTD as a function of the electron effective mass, the width and height of the barriers, and of the temperature. Moreover, we have compared three numerical algorithms and we have proposed a suitable scaling of the equations in order to have numerically stable problems.

References

1. Ancona, M.G., Iafrate, G.J.: Quantum correction to the equation of state of an electron gas in a semiconductor. Phys. Rev. B **39** (1989) 9536–9540
2. Capasso, F.: Physics of quantum electron devices. Springer Verlag, New York, 1989
3. Chen, Z., Cockburn, B., Gardner, C.L.: Quantum hydrodynamic simulation of hysteresis in the resonant tunneling diode. J. Comp. Phys. **117** (1995) 274–280
4. Jerome, J.W.: Analysis of charge transport. Springer-Verlag, New York, 1996
5. Kluksdahl, N.C., Kriman, A.M., Ferry, D.K., Ringhofer, C.A.: Self-consistent study of the resonant tunneling diode. Phys. Rev. B **39** (1989) 7720–7735
6. Lengeler, B.: Semiconductor devices suitable for use in cryogenic environments. Low temperature electronics (R.K. Kirschman ed.) IEEE, New York (1986) 62–70
7. Pinnau, R., Unterreiter, A.: The stationary current-voltage characteristics of the quantum drift-diffusion model. SIAM J. Numer. Anal. **37** (1999) 211–245
8. Simioni, P.: Modelli macroscopici con correzione quantistica per il trasporto di carica nei semiconduttori. Degree Thesis, Politecnico di Milano, 2001
9. Vinter, B., Chevoir, F.: Scattering processes, coherent and incoherent transport in resonant tunneling structures. Resonant Tunneling in Semiconductors (L. Chang ed.), Plenum Press, New York (1991) 201–211